Energy & Environmental Science

Cite this: *Energy Environ. Sci.*, 2012, **5**, 6047

www.rsc.org/ees

COMMUNICATION

Revealing the coupled cation interactions behind the electrochemical profile of $Li_xNi_{0.5}Mn_{1.5}O_4$

Eunseok Lee* and Kristin A. Persson

Received 4th November 2011, Accepted 6th January 2012
DOI: 10.1039/c2ee03068c

We present first-principles energy calculations and a cluster expansion model of the ionic ordering in $Li_xNi_{0.5}Mn_{1.5}O_4$ ($0 \leq x \leq 1$), one of the proposed high-energy density next-generation Li-ion cathode materials. The developed model predicts an intricate relationship between the preferred Li-vacancy ordering and the Ni/Mn configuration, which explains the difference in intermediate ground states between ordered ($P4_332$) and disordered ($Fd\bar{3}m$) Ni/Mn configuration. The phase sequence as a function of lithiation as well as the voltage profile are well matched with experimental results. Understanding of the inherent chemical interactions and their impact on the performance of an energy storage material is essential when designing and optimizing Li-ion electrode materials.

Li-ion batteries are poised to power the new generation of electric vehicles and thereby enable sustainable energy transportation. Among the most promising cathode materials, the lithium manganese spinel, $LiMn_2O_4$, has received attention due to its cheap price, non-toxicity, and good rate capability.[1,2] However, commercialization of $LiMn_2O_4$ has been delayed due to capacity fade upon cycling, which has been attributed to the dissolution[3–5] of Mn^{3+} produced by the redox process during lithiation/delithiation cycling.[6,7] Furthermore, it has been speculated that the strong Jahn–Teller distortion of the Mn^{3+} ion degrades the structural stability of the material and inhibits Li migration.[8–10]

Previous studies (see for example ref. 3 and references therein) aimed at improving the cycling performance by substituting other transition metals into $LiMn_2O_4$ suggest $Li_xNi_{0.5}Mn_{1.5}O_4$ as an attractive material. In $Li_xNi_{0.5}Mn_{1.5}O_4$, the redox process occurs on the Ni site only, which prevents the creation of the Mn^{3+} cation and its related problems.[11,12] Furthermore, the reduction of Ni^{4+} to Ni^{2+} occurs at 4.7 V,[3,11–15] which increases the total energy density of $Li_xNi_{0.5}Mn_{1.5}O_4$ as compared to $LiMn_2O_4$ from 440 Wh/kg to 686 Wh/kg.[16]

Despite the promising qualities of $Li_xNi_{0.5}Mn_{1.5}O_4$ for Li-ion battery applications, some of its fundamental properties have remained unexplained. For example, 1) the origin of the voltage step at $Li_{0.5}Ni_{0.5}Mn_{1.5}O_4$ and its pronounced dependence on the cation ordering,[11,17] 2) the difference in rate capability,[11,18] and 3) the occurrence of reversible phase transitions between ordered and disordered Ni/Mn arrangement during charge/discharge cycling[1,19,20] are debated. Properties such as these provide the foundation for the long-time performance and we cannot rationally design or optimize electrode materials without understanding how the electrochemical signature depends on the structure and chemistry. In this communication, we present first-principles energy calculations and a coupled cluster expansion model of the ionic ordering and its effect on the electrochemical behavior of $Li_xNi_{0.5}Mn_{1.5}O_4$. In particular, the model confirms the significant effect of a preferred commensurate Li/vacancy ordering and Ni/Mn arrangement on the phase stability and resulting voltage profile.

X-Ray Diffraction (XRD) and Transmission Electron Microscopy (TEM) analysis propose that the ground state of $Li_xNi_{0.5}Mn_{1.5}O_4$ belongs to the crystal structure $P4_332$. However, differences in synthesis procedure such as high temperature calcination can lead to another crystal structure $Fd\bar{3}m$.[1,2,11,21] Fig. 1 shows one conventional unit cell of $P4_332$ which has Li at 8*a* sites, Ni at 4*b* sites, and Mn at

Environmental Energy Technologies Division, Lawrence Berkeley National Laboratory, Berkeley, California, USA. E-mail: eunseoklee@lbl.gov

Broader context

Rechargeable Li-ion batteries have become the prime candidate for enabling electrification of the transportation sector. However, there is an increasing demand for higher energy density and power as well as lower cost associated with the active materials. Currently, the cathode presents the bottleneck in terms of energy density and considerable effort is being devoted to understanding and developing improved or new positive electrode materials. The spinel cathodes are excellent candidates because of their structural stability and high rate capability. We used first-principles calculations and analyses on a next-generation cathode spinel to elucidate and exemplify the relationship between cation interactions, structure and phase stability. Our work unravels the complicated coupling between the Li arrangement and the underlying cation lattice which provides a link between cationic interactions, the synthesis conditions of the material and its performance as an energy storage medium.

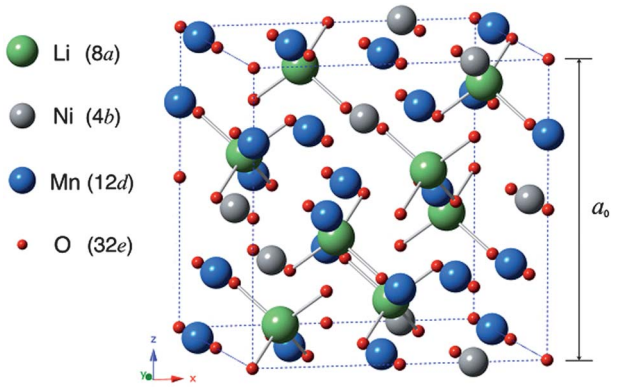

Fig. 1 One conventional cell of $Li_xNi_{0.5}Mn_{1.5}O_4$ ($P4_332$). 8*a* sites form tetrahedral structures and 4*b* and 12*d* sites form octahedral structures with the nearest neighboring oxides. a_0 is the lattice parameter.

12*d* sites (ordered), while $Fd\bar{3}m$ has Ni and Mn distributed randomly at any of the 4*b* and 12*d* sites (disordered). When the Li is extracted, the corresponding tetrahedral sites become vacant (labeled 'VA' later). By comparing the energy for different ionic configurations (Li or VA and Ni or Mn), we can identify the preferred ionic configuration in $Li_xNi_{0.5}Mn_{1.5}O_4$.

The energy is calculated by first-principles, based on zero-temperature density functional theory (DFT) within the Perdew–Burke–Ernzerhof parametrization of the generalized gradient approximation[22,23] as implemented in Vienna *ab initio* Simulation Package.[24–27] Furthermore, Projector Augmented Wave (PAW)[28,29] potentials were used. During the relaxation, both the volume and the shape of the supercell were optimized and a high cutoff energy (520 eV) together with a *k*-point sampling, which was adjusted depending on the size of supercell, ensured an energy convergence of 1 meV per atom. Spin-polarized calculations were performed to calculate the energy using different magnetic orderings. The +U scheme is employed to account for the electron localization around the transition metal ions and to calculate accurate oxidation states of Mn and Ni. In this study, we use 5.96 and 4.5 as U values of Ni and Mn, respectively.[30] The oxidation state of each ion is determined by integrating local magnetic moment within the Wigner-Seitz radius for each ion as given by the PAW potentials.

To calculate the energy for all possible cation orderings using DFT is computationally very expensive and the information obtained often redundant. Instead, we systemically select representative samples of the ionic configurations and represent the energy of the system at any ordering using a cluster expansion method. The ionic configuration of a system can be translated by the occupation variable σ_i at each lattice site *i* similar to a spin configuration of an Ising model assigning +1 to Li, −1 to VA, +1 to Mn, and −1 to Ni. In this way, the energy as a function of $\{\sigma_i\}$ is expanded by cluster functions Φ_α over all ionic clusters α's in the system, where Φ_α is defined as the product of all the spins in cluster α:

$$E(\{\sigma_i\}) = \sum_\alpha X_\alpha \Phi_\alpha(\{\sigma_i\}) \quad (1)$$

The coefficient X_α is called the effective cluster interaction (ECI) for cluster α and is fitted to existing DFT data sets. Once the ECIs are fitted, the energy of any given ionic configuration can be predicted by eqn (1). Since robust fitting requires the number of necessary DFT data sets to be greater or equal to the number of ECIs, the clusters are grouped based on the translational and rotational symmetries to reduce the number of ECIs. For further truncation, a Monte Carlo algorithm is used to select relevant clusters by minimizing the cross-validation (CV) score.[31,32] The ground state ionic configuration is searched by an iteration of fitting ECIs to existing DFT data sets and predicting the lowest energy configuration, until the newly predicted configuration and its energy already exists in DFT data sets used in the fitting. We refer the reader to ref. 32 for further details of the cluster expansion method.

At the fully lithiated state of $P4_332$, we predict that a ferrimagnetic† ordering has lower energy than the ferromagnetic ordering by 25 meV per formula unit (FU), which agrees with experimental observations.[33,34] Our calculations also reproduce the oxidation states Mn^{4+} and Ni^{2+} at fully lithiated state and we find that only the oxidation state of Ni changes during cycling. The predicted lattice parameter is 8.32 Å and 8.17 Å for the fully lithiated state and fully delithiated state, respectively. Although the lattice parameter is overestimated by 2%, its change of 1.8% during the lithiation/delithiation cycling matches well experimental observations.[20,35] The distance between the nearest neighbor Mn^{4+} ions is 2.94 Å and 2.89 Å for the fully lithiated state and fully delithiated state, respectively. Interestingly, we find that the overestimation of the Mn^{4+}–Mn^{4+} distance coupled with the localization of the Mn orbitals result in a ferromagnetic ground state of the fully delithiated state rather than an antiferromagnetic one as observed in experiments.[35,36] The failure to recapture the correct antiferromagnetic state at complete delithiation leads to a change in energy associated with a magnetic phase transition which we believe is an artifact of the overestimated volume. Hence for the fully delithiated state, we derive the ground state energy from an extrapolation of the energy in low Li content region instead from a direct DFT calculation.

The cluster expansion method is used to search the ground state Ni/Mn configuration at fully lithiated state. We find that a total of 15 different Ni/Mn configurations are needed through fitting-predicting for the cluster expansion to converge. The selected relevant clusters and the corresponding ECIs, given in the Table 1, yield a CV score of 13 meV/FU and a root-mean-square error of 12 meV/FU. We observe that the most influential cluster ('cluster 1') consists of two octahedral sites in the nearest neighbor relationship (1nn) and its positive ECI suggests a strong 1nn ordering of Ni and Mn. The predicted ground state (at 0 *K*) is $P4_332$, which agrees with the experimental observations that $Fd\bar{3}m$ is predominantly observed after annealing at higher temperatures $T > 700$ °C.[1,11]

The cluster expansion method is also used to predict the ground state Li/VA configuration for each Li content *x* in $P4_332$ and $Fd\bar{3}m$.

Table 1 Selected relevant clusters and their corresponding ECIs to predict the contribution from Ni/Mn ordering to the total energy at fully lithiated state. Empty cluster (not listed) is also selected and provides a constant. For example, the energetic contribution of a Ni and Mn pair in 'cluster 1' will be 0.2084 × 1 (Mn) × −1 (Ni), which is favorable to reduce the total energy

No.	Coordinates (a_0/8)	ECI (eV)
1	(6,0,0), (4,2,0)	0.2084
2	(6,0,0), (0,4,2)	−0.0397
3	(6,0,0), (4,2,0), (4,0,2)	−0.0632

Since there exist a tremendous number of Ni/Mn configurations, it is not possible to model $Fd\bar{3}m$ completely. Instead, in this study, we sample four physically very different Ni/Mn configurations which are labelled 'uniform', 'almost-ordered', 'segregated', and 'random'. 'Uniform' corresponds to a uniform distribution of Ni to form the face-centered-cubic Ni sublattice, 'almost-ordered' places all Ni at 4*b* sites except for one Ni per 16 FU, 'segregated' has all Ni segregated, and 'random' corresponds to *one* snap-shot configuration of randomly selected sites for Ni within the 32 transition metal supercell. We emphasize that, among the disordered configurations, the 'uniform' configuration exhibits the highest entropy and therefore corresponds to the most realistic representation of a completely disordered high temperature compound. We assume that the Ni/Mn configuration remains during charge/discharge cycling and hence the degree of freedom in a given Ni/Mn ordering is reduced to the Li/VA configuration only.

The formation energy E^I_f for each Ni/Mn configuration I is defined as $E^I_f(x) = E^I(x) - (1-x)E^I(0) - xE^I(1)$, where $E^I(x)$ is the energy of $Li_xNi_{0.5}Mn_{1.5}O_4$ of a Ni/Mn configuration I. We include the DFT data sets on or close to the convex hull of the formation energy at each iteration of fitting-predicting of the cluster expansion, as data sets with large offset from the convex hull typically degrades the fitting and results in less robustly fitted ECIs. Although E^I_f is calculated within the realm of a Ni/Mn configuration I, the entire data sets from all Ni/Mn configurations are included in the fitting of the ECIs in eqn (1) as the ECI of a certain cluster is the same in any Ni/Mn configuration.

A total of 251 DFT data sets are included when the iteration converges. The energy is predicted with a CV score of 13 meV/FU and a root-mean-square error of 12 meV/FU. The selected relevant clusters and corresponding ECIs are provided in the Table 2. Since the ECI of the empty cluster is simply a background constant, we dismiss it here. The strong negative ECI of the tetrahedral point cluster ('cluster 1') indicates that the total energy decreases with lithiation. The remarkably large positive ECI of 'cluster 2' implies the preference of a Li–VA pair for 1nn tetrahedral sites. Conversely, the negative ECI of 'cluster 3' indicates that either a Li–Li or a VA–VA arrangement for 2nn tetrahedral sites reduces the total energy. Combining the 'cluster 2' and the 'cluster 3' suggests that the most favored Li/VA configuration has the ordering of Li–VA–Li–VA–… along consecutive 1nn tetrahedral sites in a zigzag pattern as illustrated in Fig. 2. We note that the effect of this ordering on the total energy is maximized when half of the tetrahedral sites are occupied by Li, *i.e.* at $x = 0.5$.

Table 2 Selected relevant clusters and their corresponding ECIs to predict the contribution from Li/vacancy ordering to the total energy. Empty cluster (not listed) is also selected. 'T' and 'O' indicate the tetrahedral sites and the octahedral sites, respectively

No.	Coordinates (a_0/8)	ECI (eV)
1	T (1,1,1)	−3.2178
2	T(1,1,1), T(3,3,3)	0.0560
3	T(1,1,1), T(5,1,5)	−0.0079
4	T(1,1,1), T(3,3,3), O(4,2,0)	−0.0093
5	T(1,1,1), T(3,3,3), O(6,2,2)	−0.0056
6	T(1,1,1), O(6,0,0), O(6,2,2)	−0.0075
7	T(1,1,1), O(4,2,0), O(0,4,2)	−0.0036

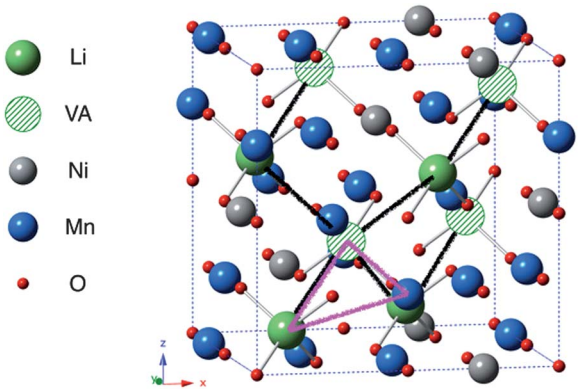

Fig. 2 Illustration of the most favored Li/VA configuration and its incompatibility with $P4_332$. Black lines indicate the zig-zag pattern of Li–VA–Li–VA–… in the most favored Li/VA configuration. Note that this Li/VA configuration is derived from the clusters composed of exclusively the tetrahedral sites. The pink triplet corresponds to one 'cluster 4' configuration.

The stability of a certain overall ionic configuration depends on the commensurateness of this favored Li/VA ordering with a given Ni/Mn configuration. Xia *et al.*[11] speculated that the Li/VA ordering at $x = 0.5$ is less commensurate with the Ni/Mn distribution in $P4_332$ than $Fd\bar{3}m$ to explain the smaller voltage step at $x = 0.5$ in $P4_332$ than $Fd\bar{3}m$. Our cluster expansion model quantitatively demonstrates this incompatibility between the ordered $P4_332$ and the preferred Li/VA ordering. For example, either the $(4,2,0)\,\frac{a_0}{8}$ site or the $(4,0,2)\,\frac{a_0}{8}$ site in Fig. 2 can form 'cluster 4' with the $(1,1,1)\,\frac{a_0}{8}$ site and the $(3,3,3)\,\frac{a_0}{8}$ site. Since both the $(4,2,0)\,\frac{a_0}{8}$ site and the $(4,0,2)\,\frac{a_0}{8}$ site are occupied by Mn in $P4_332$, the negative ECI of 'cluster 4' induces the $(1,1,1)\,\frac{a_0}{8}$ site and the $(3,3,3)\,\frac{a_0}{8}$ site to prefer Li–Li or VA–VA arrangement to reduce the total energy, which violates the favored Li/VA ordering.

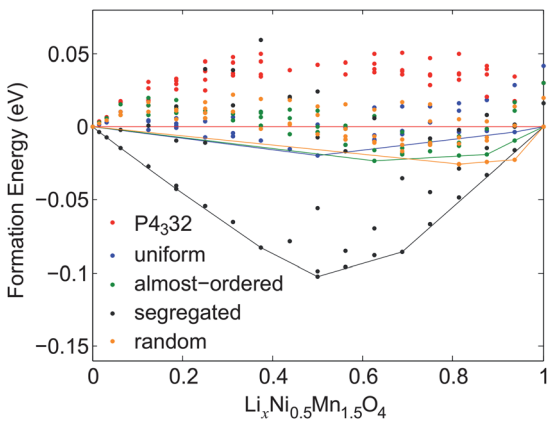

Fig. 3 Formation energy as a function of Li content x. Each point corresponds to the DFT energy calculation of a ionic configuration included in the fitting-predicting of cluster expansion method. Each continuous line shows the convex hull of the formation energy of each Ni/Mn configuration.

We can compare the effect of the ordering on the total energy from the difference in $E'(x) - E'(0)$, which is calculated at $x = 0.5$ as −3.2250, −3.2402, −3.2273, −3.1397, and −3.2329 (eV/FU) for $P4_332$, 'uniform', 'almost-ordered', 'segregated', and 'random', respectively. Except the 'segregated', which is a rather unrealistic structure, all disordered configurations exhibit Ni/Mn orderings that are more compatible with the favored Li/VA ordering than 'ordered' $P4_332$. In addition, more disordered configurations ('uniform' and 'random') are more favorable than the 'almost-ordered', which has almost the same Ni/Mn configuration as $P4_332$ except for only one Ni and one Mn per 16 FU.

Fig. 3 shows the formation energy as a function of Li content x for different Ni/Mn configurations. We find that $P4_332$ has no stable Li/VA configurations for $0 < x < 1$ (in agreement with Xia *et al.*[11]) while the disordered configurations exhibit several intermediate stable Li/VA configurations for $x \geq 0.5$. The voltage profile reflects the sequence of stable phases. We calculate the voltage as a function of x from the difference in Li chemical potential between the cathode and the anode. The calculated voltage, as well as experimental results from ref. 1, are shown in Fig. 4. The voltage profile exhibits a pronounced plateau around 4.65 V in agreement with experimental observations.[3,11–15] A constant voltage for all x in $P4_332$ is compatible with the experimental observations that the voltage step at $x = 0.5$ is negligible in $P4_332$ compared with $Fd\bar{3}m$.[11,19] We speculate (as in agreement with Xia *et al.*) that the small voltage step in $P4_332$ in some experiments may be due to small partial cation disorder in the measured samples.

Between $x = 0$ and $x = 0.5$, our investigation finds that the constant voltage is due to a two-phase region and is expected in both $P4_332$ and $Fd\bar{3}m$ (except the unrealistic 'segregated'). For perfectly uniform disordered $Fd\bar{3}m$, we predict another two-phase region between the $x = 0.5$ and $x = 1$ ordered states and a resulting voltage step at $x = 0.5$. While our zero temperature calculations yield an abrupt voltage step, we expect the step will be smoother at room temperature due to local disorder. For partially ordered/disordered arrangements ('random', 'almost-ordered') we observe a series of voltage steps for $x > 0.5$. While these two 'snap-shot' configurations will never be representative of a whole sample, they demonstrate the influence of local deviations from perfectly ordered and disordered ('uniform') samples, which will manifest in a more sloping voltage at higher lithium content. The existence of one or several two-phase regions has been reported in several previous experimental works.[1,11,19,20] Based on the analysis of the XRD and *ex-situ* TEM images, the two-phase regions has also been explained by the possibility of a topotatic phase transformation during charge/discharge cycling, *i.e.* the possible migration of cations (Ni and Mn) during the cycling.[19,20] While Ni^{2+} may be mobile, the high Li content corresponding to the oxidation state Ni^{2+} leaves insufficient vacant tetrahedral sites.[15] Based on our calculations, we propose that $P4_332$ exhibits one two-phase region which is due to the mixture of two different Li ordered states, *e.g.* $Li_0Ni_{0.5}Mn_{1.5}O_4$ and $LiNi_{0.5}Mn_{1.5}O_4$.

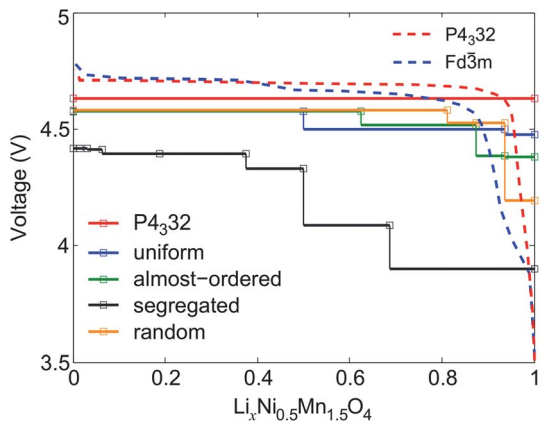

Fig. 4 Voltage as a function of Li content x - the energies along the convex hulls in Fig. 3 are used to obtain the voltage. Dashed lines are experimental observations reproduced from ref. 1.

In summary, we have developed a model to unravel the intricate cationic ordering in $Li_xNi_{0.5}Mn_{1.5}O_4$ by combining first-principles calculations with the cluster expansion method. Our findings explain the different features in the voltage profile for $P4_332$ as compared to $Fd\bar{3}m$ as a result of coupled Ni/Mn and Li/VA orderings. We quantitatively demonstrate the incommensurateness between the preferred Li/VA configuration and the Ni/Mn configuration in $P4_332$, which explains the observed negligible voltage step at $x = 0.5$ in $P4_332$ compared with $Fd\bar{3}m$. Furthermore, the predicted formation energy and the voltage as a function of Li content show that perfectly ordered $P4_332$ exhibits only one two-phase region in entire range of $0 < x < 1$, while uniformly disordered $Fd\bar{3}m$ exhibits two pronounced two-phase regions of $0 < x < 0.5$ and $0.5 < x < 1$ with the possibility of more ground states at high lithiation depending on the existence of local deviations from the overall Ni/Mn ordering. In conclusion, we have studied the influence of cation order on the Li/VA configuration and resulting phase transformations during Li intercalation which provides the necessary relationship between the materials chemistry and its performance and in turn, enables rational design of the electrode material.

Acknowledgements

Work at the Lawrence Berkeley National Laboratory was supported by the Assistant Secretary for Energy Efficiency and Renewable Energy, Office of Vehicle Technologies of the U.S. Department of Energy, under Contract No. DE-AC02-05CH11231.

Notes and references

† In the ferrimagnetic configuration, the magnetic orderings of the Ni sublattice and Mn sublattice are ferromagnetic in their own sublattice but are opposite to each other to form a ferrimagnetic ordering overall.

1 J.-H. Kim, S.-T. Myung, C. S. Yoon, S. G. Kang and Y.-K. Sun, *Chem. Mater.*, 2004, **16**, 906.
2 J. Shu, T.-F. Yi, M. Shui, Y. Wang, R.-S. Zhu, X.-F. Chu, F. Huang, D. Xu and L. Hou, *Comput. Mater. Sci.*, 2010, **50**, 776–779.
3 H. Xia, S. Tang, L. Lu, Y. Meng and G. Ceder, *Electrochim. Acta*, 2007, **52**, 2822–2828.
4 Y. Xia, T. Sakai, T. Fujieda, X. Q. Yang, X. Sun, Z. F. Ma, J. McBreen and M. Yoshio, *J. Electrochem. Soc.*, 2001, **148**, A723–A729.
5 R. Benedek and M. M. Thackeray, *Electrochem. Solid-State Lett.*, 2006, **9**, A265–A267.
6 H. M. Wu, J. P. Tu, X. T. Chen, Y. Li, X. B. Zhao and G. S. Cao, *J. Solid State Electrochem.*, 2005, **11**, 173–176.
7 Y. J. Wei, L. Y. Yan, C. Z. Wang, X. G. Xu, F. Wu and G. Chen, *J. Phys. Chem. B*, 2004, **108**, 18547–18551.
8 G. Singh, S. Gupta, R. Prasad, S. Auluck, R. Gupta and A. Sil, *J. Phys. Chem. Solids*, 2009, **70**, 1200–1206.
9 C. Ouyang, S. Shi and M. Lei, *J. Alloys Compd.*, 2009, **474**, 370–374.
10 V. W. J. Verhoeven, F. M. Mulder and I. M. de Schepper, *Phys. B*, 2000, **276–278**, 950–951.

11 H. Xia, Y. S. Meng, L. Lu and G. Ceder, *J. Electrochem. Soc.*, 2007, **154**, A737.
12 M. Mohamedi, M. Makino, K. Dokko, T. Itoh and I. Uchida, *Electrochim. Acta*, 2002, **48**, 79–84.
13 M. Jo, Y.-K. Lee, K. M. Kim and J. Cho, *J. Electrochem. Soc.*, 2010, **157**, A841–A845.
14 S.-H. Park and Y.-K. Sun, *Electrochim. Acta*, 2004, **50**, 434–439.
15 J. Reed and G. Ceder, *Chem. Rev.*, 2004, **104**, 4513–4534.
16 G. Q. Liu, L. Wen and Y. M. Liu, *J. Solid State Electrochem.*, 2010, **14**, 2191–2202.
17 Y. Terada, K. Yasaka, F. Nishikawa, T. Konishi, M. Yoshio and I. Nakai, *J. Solid State Chem.*, 2001, **156**, 286–291.
18 X. Ma, B. Kang and G. Ceder, *J. Electrochem. Soc.*, 2010, **157**, A925–A931.
19 J.-H. Kim, C. S. Yoon, S.-T. Myung, J. Prakash and Y.-K. Sun, *Electrochem. Solid-State Lett.*, 2004, **7**, A216–A220.
20 K. Ariyoshi, Y. Iwakoshi, N. Nakayama and T. Ohzuku, *J. Electrochem. Soc.*, 2004, **151**, A296.
21 T.-F. Yi, Y.-R. Zhu and R.-S. Zhu, *Solid State Ionics*, 2008, **179**, 2132–2136.
22 J. P. Perdew, K. Burke and M. Ernzerhof, *Phys. Rev. Lett.*, 1997, **78**, 1396.
23 J. P. Perdew, K. Burke and M. Ernzerhof, *Phys. Rev. Lett.*, 1996, **77**, 3865.
24 G. Kresse and J. Furthmüller, *Comput. Mater. Sci.*, 1996, **6**, 15–50.
25 G. Kresse and J. Furthmüller, *Phys. Rev. B: Condens. Matter*, 1996, **54**, 11169.
26 G. Kresse and J. Hafner, *Phys. Rev. B: Condens. Matter*, 1994, **49**, 14251.
27 G. Kresse and J. Hafner, *Phys. Rev. B: Condens. Matter*, 1993, **47**, 558.
28 G. Kresse and D. Joubert, *Phys. Rev. B: Condens. Matter Mater. Phys.*, 1999, **59**, 1758.
29 P. E. Blöchl, *Phys. Rev. B: Condens. Matter*, 1994, **50**, 17953.
30 F. Zhou, M. Cococcioni, C. A. Marianetti, D. Morgan and G. Ceder, *Phys. Rev. B: Condens. Matter Mater. Phys.*, 2004, **70**, 235121.
31 E. Lee, F. B. Prinz and W. Cai, *Phys. Rev. B: Condens. Matter Mater. Phys.*, 2011, **83**, 052301.
32 P. D. Tepesch, M. Asta and G. Ceder, *Modell. Simul. Mater. Sci. Eng.*, 1998, **6**, 787.
33 N. Amdouni, K. Zaghib, F. Gendron, A. Mauger and C. Julien, *J. Magn. Magn. Mater.*, 2007, **309**, 100–105.
34 N. Biškup, J. L. Martínez, M. E. A. y de Dompablo, P. Díaz-Carrasco and J. Morales, *J. Appl. Phys.*, 2006, **100**, 093908–093908-6.
35 K. Mukai and J. Sugiyama, *Solid State Commun.*, 2010, **150**, 906–909.
36 E. Lee and K. Persson, unpublished work.